Experimental study of the effect of icing on the aerodynamics of circular cylinders - Part I: Cross flow

Demartino, Cristoforo ; Koss, Holger; Ricciardelli, Francesco

Published in:
Proceedings of the 6th European and African Wind Engineering Conference

Publication date:
2013

Experimental study of the effect of icing on the aerodynamics of circular cylinders - Part I: Cross flow

Cristoforo Demartino[1], Holger H. Koss[2], and Francesco Ricciardelli[3]

[1]Dept. of Structural Engineering, University of Naples Federico II, via Claudio 21, 80125 Naples, Italy. *cristoforo.demartino@unina.it*
[2]Dept. of Civil Engineering, Technical University of Denmark, 2840 Kgs. Lyngby, DK.
[3]DIIES, University of Reggio Calabria, Via Graziella, 89122 Reggio Calabria, Italy.

Abstract

In this paper, the effects of ice accretion due to in-cloud icing on the aerodynamics of vertical circular cylinders is examined. Aerodynamic force coefficients with varying angle of attack were found, as a function of the wind speed; ice accretions deriving from different flow velocities and temperatures are considered. The tested cylinder is a specimen of a HDPE tube used for bridge hanger protection. The wind tunnel tests shall serve as a reference, and the results can be used for the evaluation of possible aerodynamic instability phenomena. A preliminary evaluation of possible galloping instability regions is made using the Den Hartog criterion. A short description of the accretion is given as well. A parallel paper deals with the case of circular cylinders in inclined flow.

1 Introduction

Atmospheric icing is a general term for a number of processes where water either freezes in the atmosphere and sticks to objects exposed to the air, or it freezes after getting in contact with object's surface. Ice accretion is a time-dependent modification of the shape of an object, occurring on a longer time scale compared with those of any possible dynamic response. Atmospheric icing occurs in different forms: (1) *hoar frost*, which is caused by condensation of vapour, (2) *in-cloud icing*, involving the freezing of supercooled water droplets in clouds or fog, and (3) *precipitation icing*, resulting from freezing rain, drizzle, wet snow or dry snow (Farzaneh, 2008).

The influence of ice on aerodynamics has been studied mainly in the fields of electrical distribution (Farzaneh, 2008) and of aviation, with regards to its influence on the aerodynamics of wings (Lynch & Khodadoust, 2001).

Less work is available in the area of bridge engineering. In many cases, however, bridge cables have experienced problems connected to the formation of ice. For example, the Great Belt Bridge, over the three-year period 2004-2006, has been closed for 12 hours per year on average, due to falling ice, out of a total yearly average closing hours of 14.3 (Vincentsen & Jacobsen, 2006).

Some authors have investigated experimentally and numerically the phenomenon of ice accretion on circular cylinders. Koss *et al.* (2012) investigated experimentally the shape characteristics of ice accretion on circular cylinders in vertical and horizontal configuration under the specific conditions in which real life large amplitude vibration of iced bridge cables had been observed. Gjelstrup *et al.* (2012) performed static and dynamic wind tunnel tests of vertical cylinders, using simulated ice accretion reproduced employing a rapid prototyping technique.

The purpose of this research is to investigate the effects of in-cloud ice accretions on the aerodynamics of a vertical circular cylinder, having a diameter of $160\,mm$ and made of High Density PolyEthylene (HDPE) like a typical configuration of bridge hangers. Ice accretion can lead to instability phenomena. As the wind direction and the atmospheric conditions are variable in time, ice accretion can be generated in one particular condition whilst instability can occur in a different one; accordingly aerodynamic force coefficients are measured with varying angle of attack. A preliminary evaluation of the possible galloping instability regions is made using the Den Hartog criterion. A description of the accretion is given as well. A parallel paper deals with the case of inclined flow (Demartino *et al.* , 2013).

2 Wind tunnel tests

Tests were performed in the DTU/Force collaborative Technology Climatic Wind Tunnel (CWT) in Lyngby, Denmark. The wind tunnel is a closed circuit type with test section dimensions: length $\times$ width $\times$ height $= 5\,m \times 2\,m \times 2\,m$ (Georgakis *et al.* , 2009).

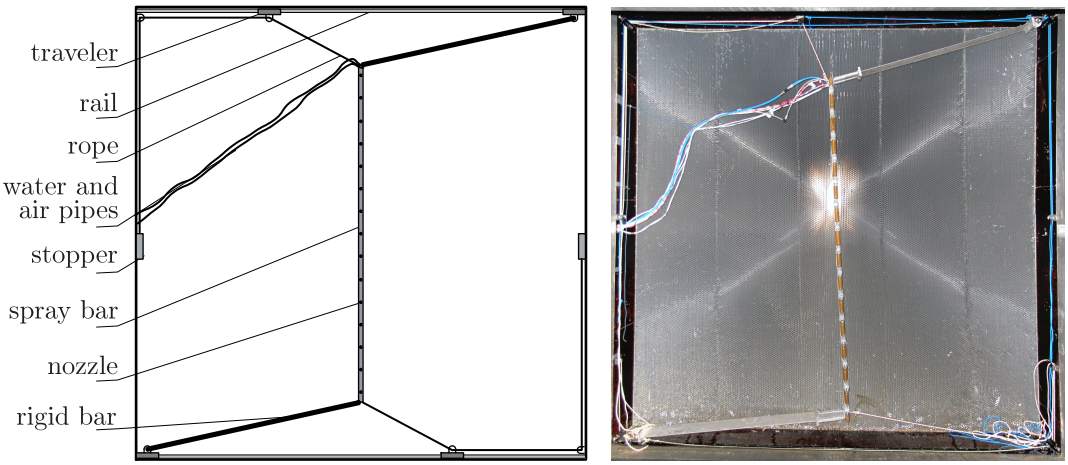

Figure 1: Spray bar suspension system: sketch (a) and photo (b).

In order to create in-cloud conditions with small super-cooled water droplets suspended in air, an assembled spray system was used in the CWT, using air atomizing spray nozzles by "Spraying Systems Co.". The spray was generated by internal mixing of water and air. The spray setup consisted of a nozzle body model 1/8J 316 SS, with a fluid cap model PF1050-316SS and a air cap model 67-6-20-70-316 SS. This configuration was able to reproduce a cloud with a median volume diameter of the droplets in the range of 10 to $80\,\mu m$, by changing the water and air pressure. The fifteen spray nozzles were mounted $20\,cm$ apart, and were connected to the air and water supply using two ring circuits. Four pressure digital sensors (Festo model SPTW-P10R-G14-VD-M12) were installed on the water and air pipes for monitoring the pressures and the variations along the circuit.

The spray system was installed in a $20\,cm \times 4\,cm \times 300\,cm$ aluminium bar. In addition heating wires were inserted inside the bar for preventing the freezing of the water when the spray system was off at temperatures below 0° Celsius. In order to streamline the spray bar, and thus reduce turbulence generation, a Plexiglas half-circle nose with a diameter of $4\,cm$ on the leading edge and a wooden tail nose on the trailing edge were added.

The spray bar was placed in the $4\,m \times 4\,m$ settling chamber directly downstream the honeycomb

grid. A support system was designed to allow rotation of the bar in the range of 0° to 90° for use in horizontal, vertical and inclined tests. The support was made of two rigid bars and two ropes respectively connected to four travelers which can move on two rails placed at the ceiling and at the floor of the settling chamber. The inclination of the spray bar was modified by changing the position of the travelers along the rails and by varying the length of the ropes. The spray bar suspension system is shown in Figure 1.

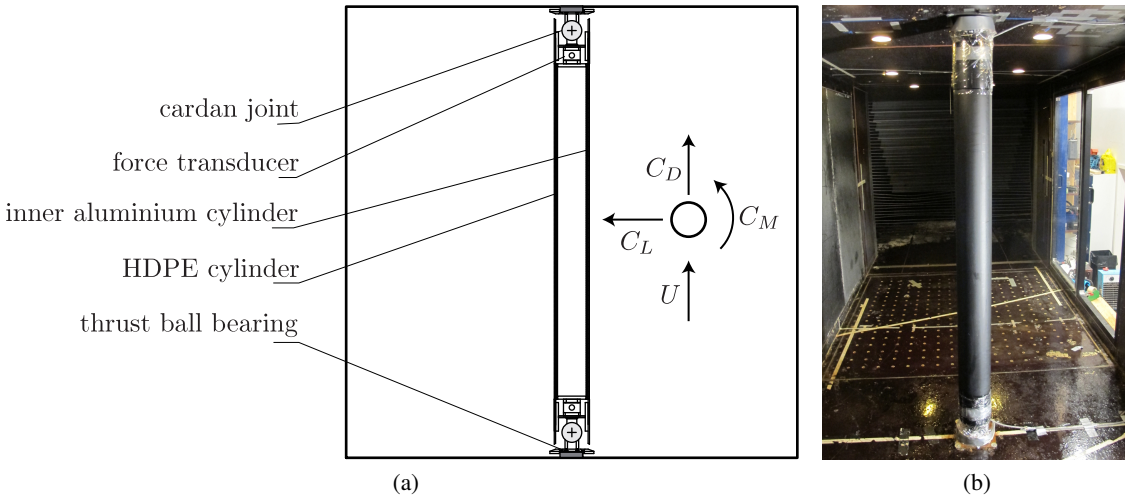

Figure 2: Cable section model setup: sketch and forces conventions (a) and photo (b).

The tested circular cylinder model was made of a plain black HDPE tube, provided by bridge cable suppliers, with a nominal diameter of $160\,mm$, stiffened with a spacer-separated inner aluminum tube. The length of the cylinder was $1.42\,m$. The model blockage ratio was 8%. Aerodynamic forces were measured at both ends of the cable using two 6-DOF force transducers (AMTI MC3A-500) installed between the cable model and the supporting cardan joints. The force transducers were covered by HDPE dummy pieces. Two thrust ball bearings were installed at both ends to allow the rotation of the cylinder. The cable model is shown in Figure 2.

Table 1: Tests and boundary condition during the ice accretion.

CC	Wind speed $[m/s]$	Temperature $[°C]$	LWC $[g/m^3]$	Mass accreted $[kg/m]$	Max accretion $[cm]$
V1	11	-5	0.2	2.4	2.9
V2	11	-3	0.2	1.5	2.1
V3	11	-1	0.2	0.6	1.4
V4	17	-5	0.3	3.0	3.5

The tests consisted of two phases: ice accretion and aerodynamic force measurements.

The control variables in the ice accretion phase were the flow velocity and the temperature. The specific Climatic Conditions (CCs) employed were: 1 hour exposure, flow velocity equal to 11 and $17\,m/s$ and temperatures equal to $-1°$, $-3°$ and $-5°$ Celsius. A summary of the tests performed is given in Table 1. The water and air pressures were set to $4.1\,bar$ and $2.5\,bar$, respectively, to obtain a droplet median diameter of $20\,\mu m$, a typical value for in-cloud icing (Poots, 1996).

In the measurement phase, the aerodynamic forces acting at different wind speeds and different angles of attack on the ice-accreted cylinder were measured. Force measurements were performed for

angles of attack in the range of $0°$ to $180°$ at intervals of $10°$ and for wind speed in the range of 8 to $29\,m/s$, at intervals of approximately $2\,m/s$. The time window used in all measurements was $30\,s$ and the sampling frequency was $2048\,Hz$. At the end of each measurement phase, the accreted ice shape was measured in a plane perpendicular to the cylinder axis.

3 Results and Discussion

3.1 Ice accretion

The main factors affecting the in-cloud ice accretion are: (i) the flow-field around the cylinder, (ii) the water droplet trajectories with subsequent impingement characteristics and (iii) the thermodynamics of the freezing/ice growth process (Lynch & Khodadoust, 2001).

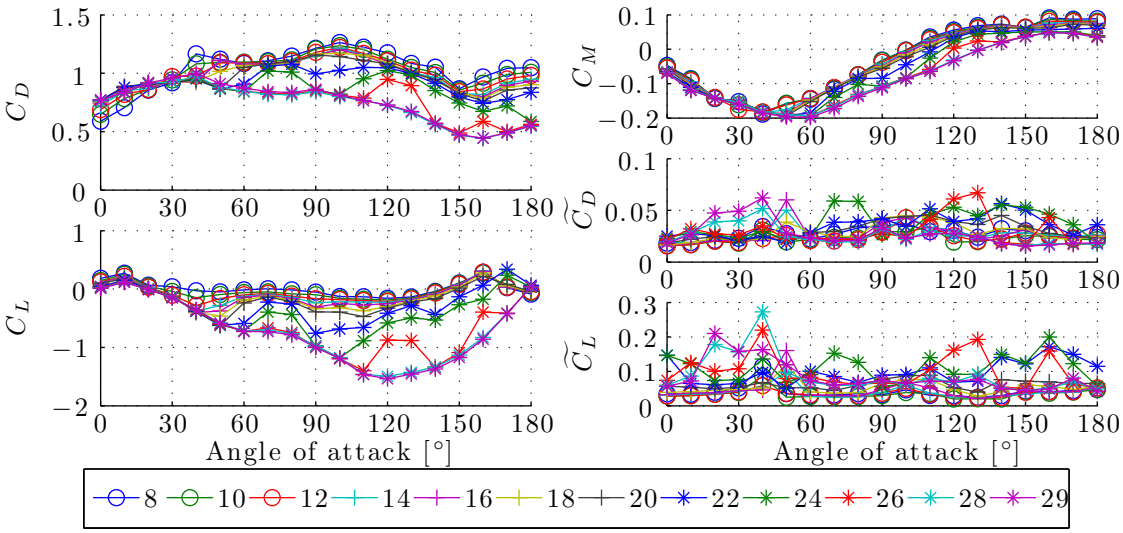

Figure 3: Variation with the angle of attack of the mean and fluctuating drag and lift coefficients and of the mean moment coefficient for wind speed of 8 to $29\,m/s$, for the ice accreted in CC V1.

The accretion can be divided in two parts: the windward accretion and the leeward accretion. The windward accretion was generated by the droplets that impact on the frontal surface of the cylinder. In this area a hard rime or glaze ice accretion was found. At the stagnation point less accretion was found in all the tests. If the water didn't freeze immediately at the contact with the surface, runback water could start from the frontal accretion area generating iced rivulets. The leeward accretion was generated by droplets that impact on the rear surface of the cylinder. The distribution in diameter of such droplets was different from that of the oncoming cloud, as only smaller droplets were deviated by the wake flow while larger ones, having higher inertia, tended to follow straighter trajectories. In this area in all CCs a soft rime was found, and the ice accreted in leeward area had low level of adhesion to the surface. During the force measurement phase the leeward part of the ice accretion was almost completely removed by the wind, when the speed was set at its maximum values. A description of the ice accretion in the frontal and lateral regions is given in Table 2.

In CC V1 the windward accretion was dominated by a hard rime and by the absence of lateral rivulets. In CC V2 the windward accretion was dominated by a hard rime combined with a moderate development of lateral rivulets. In CC V3 the windward accretion was dominated by glaze ice combined with a massive development of lateral rivulets. Finally, in CC V4 the windward accretion was again dominated by a hard rime, this time combined with a massive development of lateral rivulets.

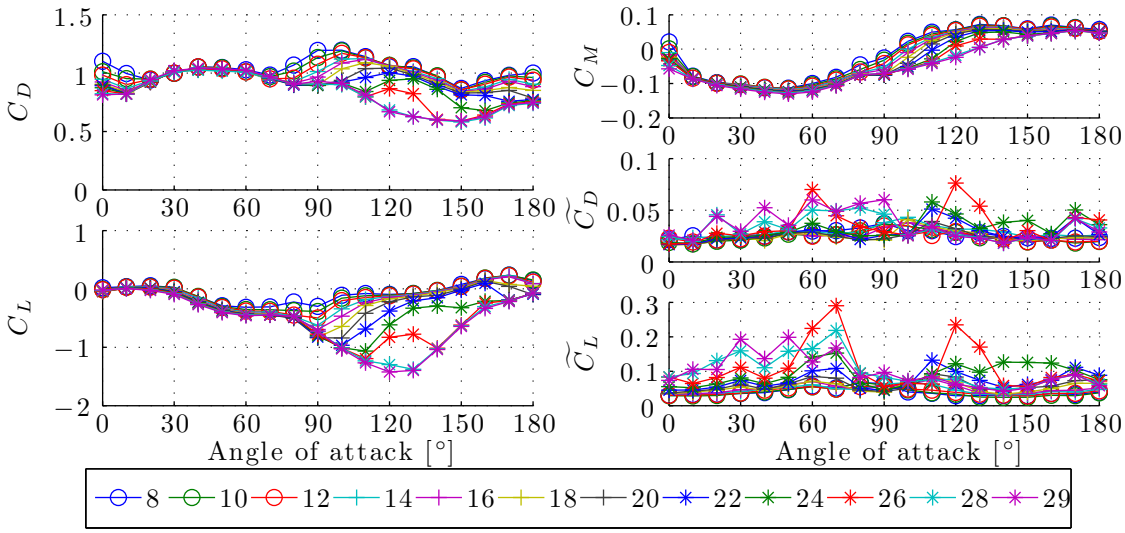

Figure 4: Variation with the angle of attack of the mean and fluctuating drag and lift coefficients and of the mean moment coefficient for wind speed of 8 to 29 m/s, for the ice accreted in CC V2.

3.2 Aerodynamic forces

The mean and fluctuating aerodynamic coefficients measured for each CC are shown in Figures 3 to 6, as a function of the angle of attack. The fluctuating aerodynamic coefficients are the standard deviation of the measured force coefficients. These were obtained rotating the cylinder about its axis. The minimum and maximum values of the mean coefficients are also given in Table 2.

Table 2: Description of the ice accretion in the frontal and lateral regions, and maximum and minimum values of the mean drag, lift and moment coefficients.

CC	Frontal accretion	Rivulet presence	Wind speed dependency	Maximum			Minimum		
				C_D	C_L	C_M	C_D	C_L	C_M
V1	High	No	30 ÷ 180°	1.29	0.33	0.09	0.44	-1.53	-0.20
V2	Mid	Low	70 ÷ 180°	1.28	0.25	0.08	0.58	-1.42	-0.13
V3	Low	High	70 ÷ 160°	1.15	0.22	0.08	0.62	-0.49	-0.08
V4	Very High	High	80 ÷ 160°	1.33	0.18	0.08	0.67	-1.33	-0.16

Globally, the aerodynamic coefficients of the accreted cylinder showed large variations with both CC and angle of attack, due to the different features of each accretion. In particular, there were situations in which the aerodynamic coefficients did not depend on wind speed, and other situations in which they did. The values of the mean aerodynamic coefficients were mainly related to the position of separation point, which was determined by the size of the frontal accretion (hard rime or glaze ice type) and by the presence, dimension and density of iced rivulets on the lateral side. The soft rime accretion on the leeward side didn't influence the aerodynamic coefficient as it was removed by the wind at high velocities.

In CC V1, for angles of attack in the range of 0° to 30°, it was found that the mean drag coefficient was only moderately dependent on wind speed, therefore on the Reynolds number. In this range it seemed that the shape of the frontal accretion determined separation from both sides of the cylinder. A similar behavior was found in the same range of angles of attack also in the other CCs. The drag coefficient for an angle of attack of 30° in CCs V1, V2 and V3 was approximately equal to 1, whilst

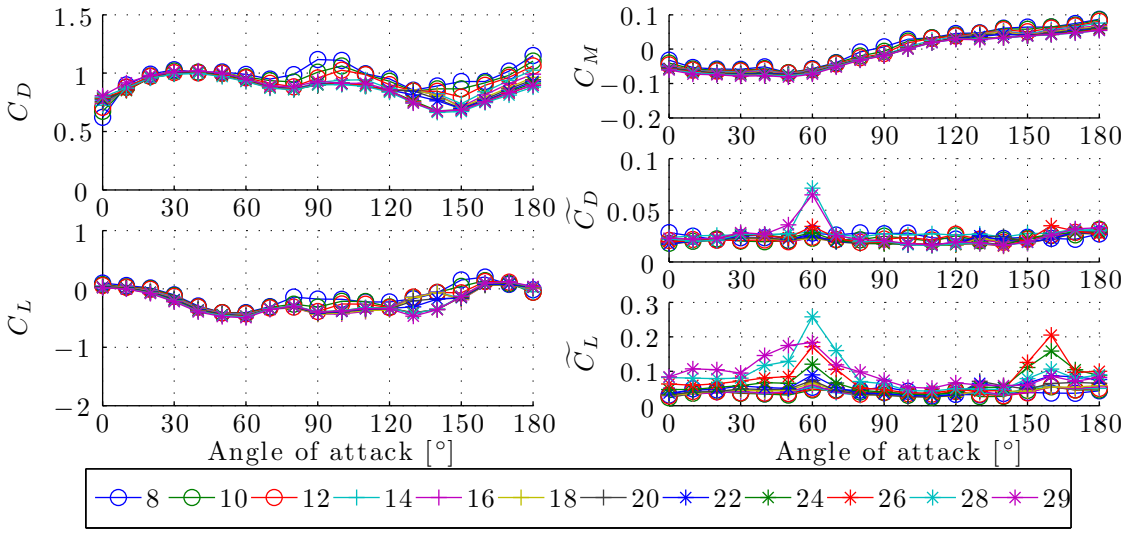

Figure 5: Variation with the angle of attack of the mean and fluctuating drag and lift coefficients and of the mean moment coefficient for wind speed of 8 to 29 m/s, for the ice accreted in CC V3.

for CC V4 it was approximately equal to 1.3. In the same range of angles of attack, the mean lift coefficient was found to be almost zero in all CCs. On the other hand, in the range of 40° to 180° a dependency of the mean drag and lift coefficients on wind speed was observed in CC V1. In this range, the maximum drag and the minimum lift were associated with the lowest wind speeds and the minimum drag and the maximum lift were associated with the highest wind speeds. Furthermore, independently of the angle of attack, the mean drag and lift coefficients were independent of the wind velocity when this was below 22 m/s and in the range of 28 m/s to 29 m/s; on the other hand the mean drag and lift coefficients showed strong variability with the wind velocity in the range of 22 m/s to 26 m/s. This behavior was observed in all CCs, and the difference from one CC to another was in the range of angles of attack in which there was a dependency of the aerodynamic forces on wind speed. In CC V1 this range was larger, whereas it was smaller in CCs V2 and V4. In CC V3 this range was similar to that of CC V4, but the dependency with respect to the wind speed was less pronounced. It can be concluded that different flow pattern exist for each CC, and that transition from one pattern to another depend on the angle of attack and on the wind speed.

In the range of 0° to 40° the moment coefficient was independent of wind speed in all CCs, and it decreased with the angle of attack, with a minimum value in the range of 40° to 60°. The smallest value of the mean moment coefficient was found in CC V1. In CC V1, in the range of 40° to 180° the mean moment started increasing, and became positive at an angle of attack of approximately 100°. In the ascending portion of the curves a dependency of the mean moment coefficient with wind velocity was found. The maximum value of the moment coefficient was reached in the range of 160° to 180°. The behavior described was found also in the remaining CCs, and the difference between one CC and another was in the range where there was a dependency of the mean moment on wind speed; these were approximately the same as those found for the mean drag and lift coefficients. The maximum value of the mean moment coefficient was approximately the same in all CCs, and, of about 0.08.

The fluctuating coefficients were found to be either constant with wind speed, or increasing with increasing wind speed. In CC V1, in the range of 0° to 30° the fluctuating coefficients were found to be increasing with wind speed, and this trend appeared not being correlated to the variation of the mean coefficients. On the other hand, in the range of 40° to 180° the largest values of the fluctuating coefficients were associated with strong variations in the mean coefficients with respect of the wind

speed, i.e. the range of $22\,m/s$ to $26\,m/s$. A similar behavior was found in the other CCs, with a slight variations in the ranges above.

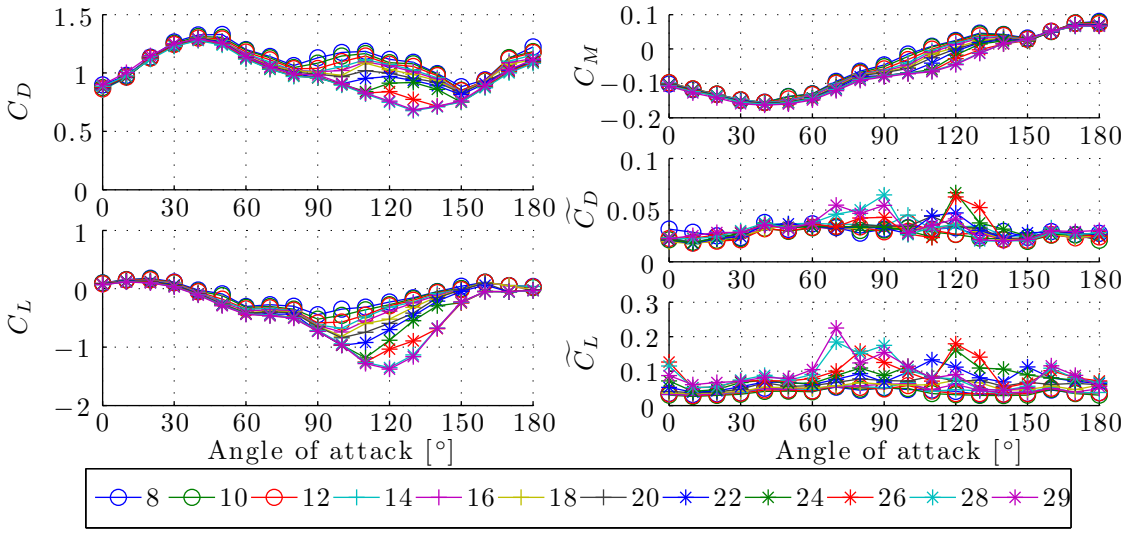

Figure 6: Variation with the angle of attack of the mean and fluctuating drag and lift coefficients and of the mean moment coefficient for wind speed of 8 to $29\,m/s$, for the ice accreted in CC V4.

3.3 Aerodynamic instability

The susceptibility of the accreted cylinder to galloping is evaluated using the Glauert-Den Hartog criterion:

$$C_D + C'_L < 0 \tag{1}$$

in which C'_L is the derivative of the mean lift coefficient respect to the angle of attack. The evaluation of Eqn. 1 is shown in Figure 7 for all CCs. In the range of $0°$ to $40°$ in all CCs a globally decreasing stability was observed. In CC V1 for angles of attack in excess of $40°$, the Glauert-Den Hartog coefficient became dependent on wind speed, due to the dependency of the mean drag and lift coefficients. A generally stable behavior was observed in CC V3 for all the wind speed, with nearly zero values for angles of attack in the range of $30°$ to $40°$. A stable behavior was observed in CCs V1, V2 and V4 for the wind speed below $18\,m/s$, while an unstable behavior has to be expected for higher wind speeds, depending on the angle of attack. A common feature of CCs V1, V2 and V4 was that an unstable behavior is indicated for angles of attack in the range of $70°$ to $110°$. These CCs were characterized by a hard rime type ice in the frontal region.

4 Conclusion

The aerodynamic force coefficients of a cylinder vertically placed in the wind tunnel were measured, simulating a vertical hanger of a suspension bridge, for different ice accretion conditions. Measurements were repeated for different wind speeds and angles of attack. The coefficients of the accreted cylinder showed considerable variations for each condition of ice accretion. This variation was due to the different features of each ice accretion. The measured aerodynamic force coefficients were used for assessing the galloping stability of the cylinder, using the Glauert-Den Hartog criterion. A negative aerodynamic damping was found only for rime type ice and for selected angles of attack.

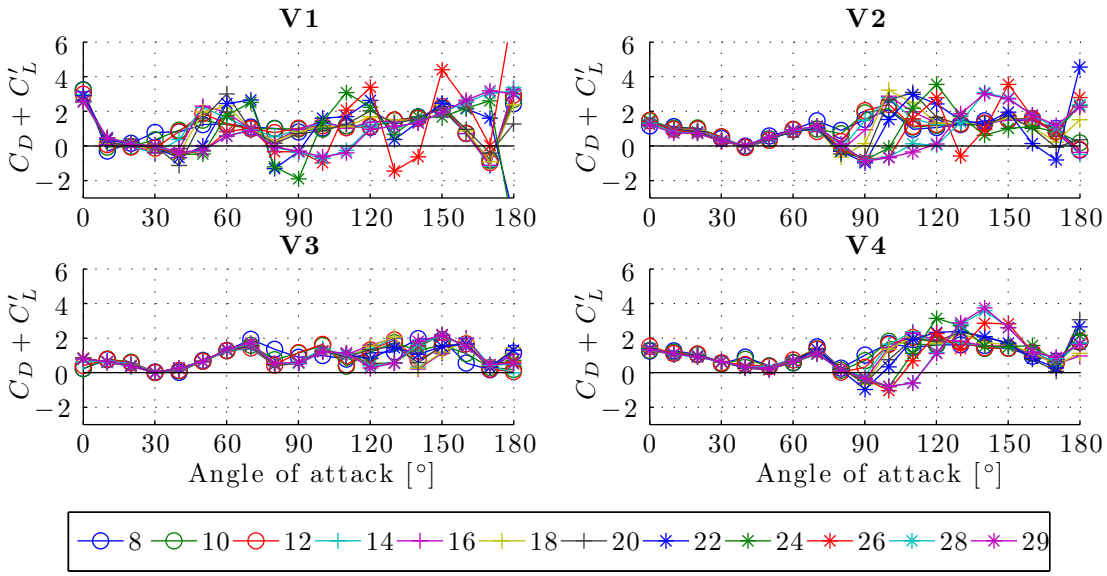

Figure 7: Glauert-Den Hartog coefficient $C_D + C'_L$ for the CCs V1 to V4.

Acknowledgements

The authors acknowledge the financial support of Storebælt A/S, Femern A/S and Force Technology, without which this work would have not been possible.

References

Demartino, C., Georgakis, C.T., & Ricciardelli, F. 2013. Experimental study of the effect of icing on the aerodynamics of circular cylinders - Part II: Inclined flow. *In: 6th European and African Conference on Wind Engineering, Cambridge*.

Farzaneh, M. 2008. *Atmospheric icing of power networks*. Springer.

Georgakis, C.T., Koss, H.H., & Ricciardelli, F. 2009. Design specifications for a novel climatic wind tunnel for testing of structural cables. *In: 8th International Symposium on Cable Dynamics, Paris*.

Gjelstrup, H., Georgakis, C.T., & Larsen, C.T. 2012. An evalution of iced bridge hanger vibrations through wind tunnel testing and quasi-stedy theory. *Wind and Structures*, **15**(5), 385–407.

Koss, H.H., Gjelstrup, H., & Georgakis, C.T. 2012. Experimental study of ice accretion on circular cylinders at moderate low temperatures. *Journal of Wind Engineering and Industrial Aerodynamics*, **104-106**, 540–546.

Lynch, F.T., & Khodadoust, A. 2001. Effects of ice accretions on aircraft aerodynamics. *Progress in Aerospace Sciences*, **37**(8), 669–767.

Poots, Graham. 1996. *Ice and snow accretion on structures*. Vol. 338. Research Studies Press.

Vincentsen, L.J., & Jacobsen, H.H. 2006. Operation and Maintenance of the Great Belt Bridge. *Pages 40–48 of: IABSE Symposium Report*, vol. 84.